Inorganic Chemistry

Article

pubs.acs.org/IC

Crystal Growth of Four Oxovanadium(IV) Tartrates Prepared via a Mild Two-Step Hydrothermal Method: Observation of Spin-Dimer Behavior and Second Harmonic Generation

Anthony J. Cortese,[†] Branford Wilkins,[†] Mark D. Smith,[†] Jeongho Yeon,[†] Gregory Morrison,[†] T. Thao Tran,[‡] P. Shiv Halasyamani,[‡] and Hans-Conrad zur Loye*[,†]

[†]Department of Chemistry and Biochemistry, University of South Carolina, Columbia, South Carolina 29208, United States

[‡]Department of Chemistry, University of Houston, Houston, Texas 77204, United States

Supporting Information

ABSTRACT: Four new oxovanadium(IV) tartrates, namely, $A_2[(VO)_2(C_4H_4O_6)(C_4H_2O_6)(H_2O)_2]\cdot(H_2O)_2$, where A = Cs, **1**, Rb, **2**; $K_2[(VO)_2(C_4H_4O_6)_2(H_2O)_2]\cdot(H_2O)_2$, **3**; and $Na_2[(VO)_2(C_4H_4O_6)(C_4H_2O_6)(H_2O)_7]\cdot(H_2O)_2$, **4**, were prepared utilizing a two-step, mild hydrothermal route involving L-(+)-tartaric acid as the reducing agent. All four compounds were structurally characterized by single-crystal and powder X-ray diffraction methods and were found to crystallize in the non-centrosymmetric orthorhombic space groups $P2_12_12_1$ for **1**, **2**, and **4** and $C222_1$ for **3**. The temperature dependence of the magnetic susceptibility of these compounds was measured, and **1**, **2**, and **4** were found to be paramagnetic down to 2 K, while **3** was found to exhibit spin-dimer behavior. Compounds **1**, **2**, and **3** were found to be second harmonic generation active. All compounds were further characterized by IR and UV−vis spectroscopies.

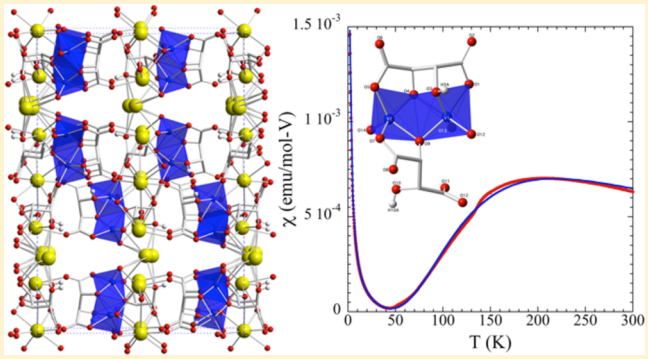

INTRODUCTION

Vanadium-containing compounds have been investigated for a variety of applications, including as magnetic materials,[1−4] for catalysts,[5−8] as cathode materials,[9−12] and as ion-exchange materials.[13,14] In these applications the vanadium oxidation state can range from fully oxidized, as in some oxidation catalysts, to reduced, as in some lithium battery cathode materials. Overall, the oxidation state chemistry of vanadium is rich and includes the +5, +4, +3, and +2 oxidation states, where color is often used to distinguish and confirm the oxidation states of vanadium species. In an aqueous environment, vanadium can exist in oxidation states ranging from +2 to +5 with colors ranging from yellow (V^{5+}), blue (V^{4+}), and green (V^{3+}) to lilac (V^{2+}).[15−21] It is possible to reduce aqueous vanadium species using organic reducing agents, where the combination of organic reagent and temperature determine the final vanadium oxidation state. While harsher conditions, such as sulfuric acid-catalyzed zinc reduction under inert atmosphere, are needed to create V^{2+} in aqueous solutions, many simple organic acids, including oxalic acid, citric acid, ascorbic acid, and tartaric acid, can be used to create V^{4+} in solution.[20,21] One such acid, tartaric acid, has the ability to perform the reduction of vanadium from +5 to +4 in air under mild hydrothermal conditions. With both carboxyl and hydroxyl functional groups and a flexible carbon backbone, tartaric acid is an attractive candidate as a ligand for vanadium containing hybrid materials owing to the variety of chelating motifs that can be adopted. A few vanadium−tartrate hybrid materials are known, including $[Sr(VO)((\pm)\text{-}C_4H_2O_6)(H_2O)_3]_2$,[22] $A_4[(VO)(C_4H_2O_6)]_2\cdot xH_2O$ A = Cs, Rb,[23] $Na_4[V_4O_8((\pm)\text{-}C_4H_2O_6)_2]\cdot(H_2O)_{12}$,[24] and $(N(CH_2CH_3)_4)[V_4O_8(D\text{-}C_4H_2O_6)_2]\cdot(H_2O)_6$.[24]

We recently reported on a convenient two-step hydrothermal method that facilitates the formation of hybrid materials containing metal cations in reduced states.[21,25] In the case of reactions where the rate of vanadium reduction is slow relative to the crystallization of an unwanted species, either V^{5+}-containing complexes or mixed-ligand complexes, the use of the two-step approach is extremely effective for obtaining the desired V^{4+} products. Essentially the reduction step and the product creation step are performed sequentially. In the first step the vanadium cation is reduced from +5 to +4, and in the second step, the crystallization of the hybrid material takes place. This is a completely general approach that can be extremely helpful for many reactions where the simultaneous *in situ* reduction and complex formation does not succeed due to unfavorable kinetics of competing crystallization processes.

To create the title compounds $A_2[(VO)_2(C_4H_4O_6)(C_4H_2O_6)(H_2O)_2]\cdot(H_2O)_2$, where A = Cs, Rb, and $K_2[(VO)_2(C_4H_4O_6)_2(H_2O)_2]\cdot(H_2O)_2$, we used this two step approach

Received: February 4, 2015
Published: March 31, 2015

DOI: 10.1021/acs.inorgchem.5b00275
Inorg. Chem. 2015, 54, 4011−4020

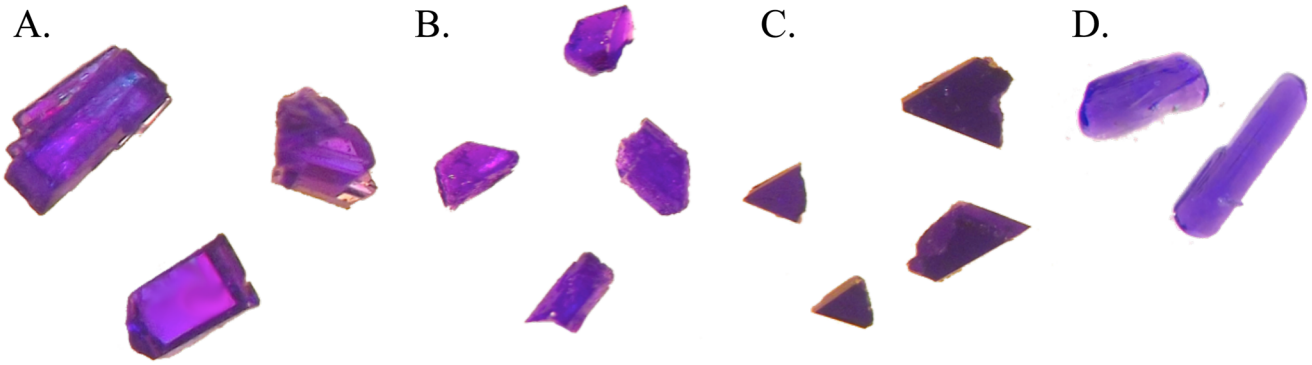

Figure 1. Optical image of single crystals of (A) $Cs_2[(VO)_2(C_4H_4O_6)(C_4H_2O_6)(H_2O)_2]\cdot(H_2O)_2$, (B) $Rb_2[(VO)_2(C_4H_4O_6)(C_4H_2O_6)(H_2O)_2]\cdot(H_2O)_2$, and (C) $K_2[(VO)_2(C_4H_2O_6)_2(H_2O)_2]\cdot(H_2O)_2$. Crystals are ~0.75 mm in length.

and sequentially performed the vanadium reduction step and the crystallization of the vanadium−L-(+)-tartaric acid-containing product step. To create $Na_2[(VO)_2(C_4H_4O_6)(C_4H_2O_6)(H_2O)_7]\cdot(H_2O)_2$, a slow evaporation method was employed. The use of enantiomerically pure tartaric acid in the syntheses to create tartaric acid-containing products will, by default, create enantiomerically pure chiral materials. Consequently, the four title compounds are all chiral and, therefore, non-centrosymmetric, which is one of the requirements for materials to display second harmonic generation (SHG). Compounds crystallizing in non-centrosymmetric space groups are capable of exhibiting interesting nonlinear optical properties including piezoelectricity, pyroelectricity, circular dichroism, and SHG.[26] The title compounds all crystallize in non-centrosymmetric orthorhombic space groups allowing for the measurement of their SHG response.

Using the two-step reduction method we successfully synthesized four new chiral oxovanadium(IV) tartrates in good yield. Herein we report the synthesis, structural characterization, magnetic properties, and SHG response of these compounds.

EXPERIMENTAL SECTION

Reagents. V_2O_5 (99.6% min, Alfa Aesar), L-(+)-$C_4H_6O_6$ (99%, Alfa Aesar), CsCl (99%, Alfa Aesar), Cs_2CO_3 (99%, Alfa Aesar), RbCl (99%, Alfa Aesar). Rb_2CO_3 (99%, Alfa Aesar), KCl (Certified A.C.S., Fisher) K_2CO_3 (Certified A.C.S., Fisher), NaCl (Certified A.C.S., Fisher), Na_2CO_3 (Certified A.C.S., Fisher), methanol (Certified A.C.S., BDH), and ethanol (USP Spec, Decon Laboratories, Inc.) were used as received.

Synthesis. *$Cs_2[(VO)_2(C_4H_4O_6)(C_4H_2O_6)(H_2O)_2]\cdot(H_2O)_2$*, ***1***. Purple colored single crystals of $Cs_2[(VO)_2(C_4H_4O_6)(C_4H_2O_6)(H_2O)_2]\cdot(H_2O)_2$, **1**, were grown via a two-step hydrothermal route. In the first step, 1 mmol of V_2O_5, 4 mmol of L-(+)-$C_4H_6O_6$, and 4 mL of H_2O were placed in a poly(tetrafluoroethylene) (PTFE) autoclave. The autoclave was placed inside a programmable oven and heated to 160 °C at a rate of 10 °C/min, held for 4 h, and cooled to room temperature by turning off the oven. The resulting blue solution was reacted with 2 mmol of Cs_2CO_3 and 3 mmol of CsCl and added to a thick-walled PTFE-capped Pyrex tube. The tube was placed inside a programmable oven and heated to 90 °C at a rate of 10 °C/min, held for 48 h, and cooled to room temperature at a rate of 0.1 °C/min. The mother liquor was decanted yielding a phase-pure product in ~85% yield based on V_2O_5. Figure 1 shows an optical image of **1**. A powder X-ray diffraction (PXRD) pattern of ground crystals demonstrates the phase purity of the product crystals. Supporting Information, Figure S1.

$Rb_2[(VO)_2(C_4H_4O_6)(C_4H_2O_6)(H_2O)_2]\cdot(H_2O)_2$, ***2***. Purple colored single crystals of $Rb_2[(VO)_2(C_4H_4O_6)(C_4H_2O_6)(H_2O)_2]\cdot(H_2O)_2$, **2**, were grown via a two-step hydrothermal route. In the first step, 1 mmol of V_2O_5, 4 mmol of L-(+)-$C_4H_6O_6$, and 4 mL of H_2O were placed in a PTFE autoclave. The autoclave was placed inside a programmable oven and heated to 160 °C at a rate of 10 °C/min, held for 4 h, and cooled to room temperature by turning off the oven. The resulting blue solution was reacted with 2 mmol of Rb_2CO_3, 3 mmol of RbCl, and 2.7 mL of ethanol and added to a thick-walled PTFE-capped Pyrex tube. The tube was placed inside a programmable oven and heated to 90 °C at a rate of 10 °C/min, held for 48 h, and cooled to room temperature at a rate of 0.1 °C/min. The mother liquor was decanted yielding a phase-pure product in ~80% yield based on V_2O_5. Figure 1 shows an optical image of **2**. A PXRD pattern of ground crystals demonstrates the phase purity of the product crystals. Figure S1.

$K_2[(VO)_2(C_4H_2O_6)_2(H_2O)_2]\cdot(H_2O)_2$, ***3***. Purple colored single crystals of $K_2[(VO)_2(C_4H_2O_6)_2(H_2O)_2]\cdot(H_2O)_2$, **3**, were grown via a two-step hydrothermal route. In the first step, 1 mmol of V_2O_5, 4 mmol of L-(+)-$C_4H_6O_6$, and 4 mL of H_2O were placed in a PTFE autoclave. The autoclave was placed inside a programmable oven and heated to 160 °C at a rate of 10 °C/min, held for 4 h, and cooled to room temperature by turning off the oven. The resulting blue solution was reacted with 2 mmol of K_2CO_3, 3 mmol of KCl, and 1 mL of methanol and added to a thick-walled PTFE-capped Pyrex tube. The tube was placed inside a programmable oven and heated to 90 °C at a rate of 10 °C/min, held for 48 h, and cooled to room temperature at a rate of 0.1 °C/min. The mother liquor was decanted yielding a phase pure product in ~75% yield based on V_2O_5. Figure 1 shows an optical image of **3**. A PXRD pattern of ground crystals demonstrates the phase purity of the product crystals. Figure S1.

$Na_2[(VO)_2(C_4H_4O_6)(C_4H_2O_6)(H_2O)_7]\cdot(H_2O)_2$, ***4***. Blue colored single crystals of $Na_2[(VO)_2(C_4H_4O_6)(C_4H_2O_6)(H_2O)_7]\cdot(H_2O)_2$, **4**, were grown via a one-step hydrothermal technique followed by slow evaporation. In the first step, 1 mmol of V_2O_5, 4 mmol of L-(+)-$C_4H_6O_6$, and 4 mL of H_2O were placed in a PTFE autoclave. The autoclave was placed inside a programmable oven and heated to 160 °C at a rate of 10 °C/min, held for 4 h, and cooled to room temperature by turning off the oven. The resulting blue solution was reacted with 2 mmol of Na_2CO_3 and 3 mmol of NaCl and added to a thick-walled pyrex tube. The solution was allowed to evaporate very slowly at room temperature for 120 d. The mother liquor was decanted yielding a phase pure product in ~30% yield based on V_2O_5. Figure 1 shows an optical image of **4**. A PXRD pattern of ground crystals demonstrates the phase purity of the product crystals. Figure S1.

Single-Crystal X-ray Diffraction. X-ray intensity data from deep violet rectangular plates of **1** and **2**, a purple hexagonal plate of **3**, and a purple needle of **4** were collected at 100(2) K using a Bruker SMART APEX diffractometer (Mo Kα radiation, λ = 0.710 73 Å).[27] The raw area detector frames were reduced and corrected for absorption effects using the SAINT+ and SADABS programs.[27] Final unit cell parameters were determined by least-squares refinement of reflections from the data set. Direct methods structure solution, difference Fourier calculations, and full-matrix least-squares refinements against F^2 were performed with SHELXS and SHELXL-2013/4[28] using OLEX2.[29]

Compounds **1** and **2** are isostructural and crystallize in the orthorhombic space group $P2_12_12_1$ as determined by the pattern of

DOI: 10.1021/acs.inorgchem.5b00275
Inorg. Chem. 2015, 54, 4011−4020

Table 1. Crystallographic Data for $A_2[(VO)_2(C_4H_4O_6)(C_4H_2O_6)(H_2O)_2]\cdot(H_2O)_2$, A = Cs, 1; Rb, 2; $K_2[(VO)_2(C_4H_2O_6)_2(H_2O)_2]\cdot(H_2O)_2$, 3; and $Na_2[(VO)_2(C_4H_4O_6)(C_4H_2O_6)(H_2O)_7]\cdot(H_2O)_2$, 4

	1	2	3	4
formula weight	765.89	671.01	577.54	636.13
temperature (K)	100(2)	100(2)	100(2)	100(2)
crystal system	orthorhombic	orthorhombic	orthorhombic	orthorhombic
space group	$P2_12_12_1$	$P2_12_12_1$	$C222_1$	$P2_12_12_1$
a (Å)	8.0320(6)	7.9061(8)	8.4341(13)	8.5931(5)
b (Å)	10.4016(8)	10.2647(11)	17.311(3)	10.4332(6)
c (Å)	23.3623(17)	22.814(2)	25.140(4)	24.2289(13)
volume, Å^3	1951.8(3)	1851.5(3)	3670.5(10)	2172.2(2)
Z	4	4	8	4
density (g/cm^3)	2.61	2.41	2.09	1.95
abs coeff (mm^{-1})	4.7	6.3	1.6	1.0
R(int)	0.0437	0.0466	0.0833	0.0647
$R(F)^a$	0.0210	0.0238	0.0339	0.0398
$R_w(F_o^2)^b$	0.0478	0.0527	0.0616	0.0877
Flack parameter	0.015(14)	−0.015(5)	0.01(2)	0.025(7)

$^aR(F) = \sum||F_o| - |F_c||/\sum|F_o|$. $^bR_w(F_o^2) = [\sum w(F_o^2 - F_c^2)^2/\sum w(F_o^2)^2]^{1/2}$.

systematic absences in the intensity data and by structure solution. The asymmetric unit consists of two cesium atoms, two VO^{2+} units, two differently protonated tartrate ligands, and several coordinated and noncoordinated water molecules. One tartrate ligand (C1−C4, O1−O6) is deprotonated only at the carboxylate groups, giving it a charge of −2. The second independent tartrate ligand (C5−C8, O7−O12) is fully deprotonated at both carboxylate groups and both hydroxyl groups, giving it a charge of −4. The state of protonation of the two independent tartrate ligands was determined by (a) clear presence or absence of reasonably refinable hydrogen atoms in the Fourier difference map, enabled by the very high crystal quality of the material, (b) analysis of the hydrogen bonding environments of each candidate oxygen atom, and (c) longer bond distances from the hydroxyl oxygen atoms to vanadium. All non-hydrogen atoms were refined with anisotropic displacement parameters. Hydrogen atoms bonded to carbon were located in difference maps before being placed in geometrically idealized positions and included as riding atoms. The hydroxyl and water hydrogen atoms were located in difference maps and refined isotropically, with d(O−H) distances restrained to 0.84(2) Å. The absolute structure (Flack) parameters refined to 0.015(14), 0.015(5), and 0.025(7) for **1**, **2**, and **4**, respectively, confirming the enantiopurity of the material and that the correct absolute structure was refined.

Compound **3** crystallizes in the orthorhombic space group $C222_1$ as determined uniquely by the pattern of systematic absences in the intensity data. The asymmetric unit consists of two vanadium atoms, three potassium atoms, two of which are located on twofold axes of rotation, two singly protonated tartrate anions, and several water molecules. Potassium atoms K1 and K3 are located on C_2 axes. K3 is disordered over two sites on the C_2 axis, with occupancies K3A/K3B = 0.69(2)/0.31(2) (constrained to sum to unity). Several disordered and fractionally occupied oxygen atoms of water molecules were located in the vicinity of potassium atoms K2 and K3. The oxygens numbered O15−O17 are within reasonable distances to be considered bonded to K2 and K3. O15 was modeled with two sites, O16 was modeled with three sites, and O17 was modeled with two sites. Occupancies of O15A/B and O16A/B/C were constrained to unity. O17A/B occupancies were refined freely. Four additional peaks, O1S−O4S, are distant enough from potassium to be considered noncoordinated interstitial water molecules. Their occupancies were also refined freely. Non-hydrogen atoms were refined with anisotropic displacement parameters except for disordered oxygen atoms (isotropic). Hydrogen atoms bonded to carbon were placed in geometrically idealized positions and included as riding atoms. The two hydroxyl hydrogen atoms of the tartrate ligands (H3A and H10A) were located in difference maps and refined isotropically with their O−H distances restrained to d(O−H) = 0.84(2) Å. After the final refinement cycle, the absolute structure (Flack) parameter was 0.01(2), confirming the enantiopurity of the material and that the correct absolute structure was refined.

Compound **4** crystallizes in the orthorhombic space group $P2_12_12_1$ as determined by the pattern of systematic absences in the intensity data. The asymmetric unit consists of two sodium atoms, two VO^{2+} units, two differently protonated tartrate ligands, seven coordinated water molecules, and two noncoordinated water molecules. One tartrate ligand (C1−C4, O1−O6) is deprotonated only at the carboxylate groups, giving it a charge of −2. The second independent tartrate ligand (C5−C8, O7−O12) is fully deprotonated (both carboxylate groups and both hydroxyl groups), giving it a charge of −4. The state of protonation of the two independent tartrate ligands was determined by (a) clear presence or absence of hydrogen atoms in the Fourier difference map, (b) analysis of the hydrogen bonding environments of each candidate oxygen atom, and (c) longer bond distances from the protonated hydroxyl oxygen atoms to vanadium compared to the deprotonated hydroxyl V−O distances. All non-hydrogen atoms were refined with anisotropic displacement parameters except where noted below. Hydrogen atoms bonded to carbon were placed in geometrically idealized positions and included as riding atoms. The hydroxyl and water hydrogen atoms were located in difference maps. Most were refined isotropically with d(O−H) distances restrained to 0.84(2) Å. Those bonded to O18 and O21 were located, their distances adjusted to give d(O−H) = 0.84 Å, and subsequently refined as riding atoms with $U_{iso,H} = 1.5U_{eq,O}$. One noncoordinated water (O23) is disordered over two sites and was refined isotropically with the total site population constrained to sum to unity. The absolute structure (Flack) parameter refined to 0.025(7), confirming the enantiopurity of the material and that the correct absolute structure was refined.

Crystallographic data, selected interatomic distances, and selected hydrogen bonding distances are listed in Tables 1, 2, and 3, respectively. Bond valence sums[30,31] for vanadium were calculated for all four structures and found to be between 4.09 and 4.17,[32] confirming the oxidation state of V as +4 and being consistent with the compositions obtained by single crystal X-ray diffraction.

Powder X-ray Diffraction. PXRD data were collected on a Rigaku D/Max-2100 powder X-ray diffractometer using Cu Kα radiation. The step scan covered the angular range 5−45° 2θ in steps of 0.04°. No impurities were observed, and the calculated and experimental PXRD patterns are in excellent agreement (see Supporting Information, Figure S1).

Energy-Dispersive Spectroscopy. Elemental analysis was performed on the single crystals using a TESCAN Vega-3 SBU scanning electron microscope (SEM) with energy-dispersive spectroscopy (EDS) capabilities. The crystals were mounted on carbon tape and

DOI: 10.1021/acs.inorgchem.5b00275
Inorg. Chem. 2015, 54, 4011−4020

Table 2. Selected Interatomic Distances (Å) for $A_2[(VO)_2(C_4H_4O_6)(C_4H_2O_6)(H_2O)_2]\cdot(H_2O)_2$, A = Cs, 1; Rb, 2; $K_2[(VO)_2(C_4H_2O_6)_2(H_2O)_2]\cdot(H_2O)_2$, 3; and $Na_2[(VO)_2(C_4H_4O_6)(C_4H_2O_6)(H_2O)_7]\cdot(H_2O)_2$, 4

			1				
Cs(1)–O(2)	3.197(2)	Cs(1)–O(17)	3.753(3)	Cs(2)–O(16)	3.082(2)	V(1)–O(14)	1.606(2)
Cs(1)–O(6)	3.013(2)	Cs(2)–O(1)	3.159(2)	Cs(2)–O(17)	3.266(3)	V(2)–O(4)	2.216(2)
Cs(1)–O(8)	3.157(2)	Cs(2)–O(3)	3.071(2)	Cs(2)–O(18)	3.456(3)	V(2)–O(5)	2.010(2)
Cs(1)–O(11)	3.124(2)	Cs(2)–O(6)	3.449(3)	V(1)–O(1)	2.010(2)	V(2)–O(10)	1.969(2)
Cs(1)–O(12)	3.193(2)	Cs(2)–O(12)	3.131(2)	V(1)–O(3)	2.269(3)	V(2)–O(11)	1.991(2)
Cs(1)–O(13)	3.539(3)	Cs(2)–O(13)	3.599(3)	V(1)–O(7)	1.987(2)	V(2)–O(15)	2.074(3)
Cs(1)–O(14)	3.019(2)	Cs(2)–O(14)	3.206(3)	V(1)–O(9)	1.952(2)	V(2)–O(16)	1.608(3)
Cs(1)–O(16)	3.019(2)	Cs(2)–O(15)	3.408(3)	V(1)–O(13)	2.043(3)		
			2				
Rb(1)–O(2)	3.125(2)	Rb(1)–O(17)	3.539(2)	Rb(2)–O(16)	2.954(2)	V(1)–O(14)	1.607(2)
Rb(1)–O(6)	2.896(2)	Rb(2)–O(1)	2.997(2)	Rb(2)–O(17)	3.168(3)	V(2)–O(4)	2.200(2)
Rb(1)–O(8)	3.030(2)	Rb(2)–O(3)	2.983(2)	Rb(2)–O(18)	3.357(2)	V(2)–O(5)	2.001(2)
Rb(1)–O(11)	3.044(2)	Rb(2)–O(6)	3.357(3)	V(1)–O(1)	2.018(2)	V(2)–O(10)	1.964(2)
Rb(1)–O(12)	2.986(2)	Rb(2)–O(12)	2.999(2)	V(1)–O(3)	2.275(2)	V(2)–O(11)	1.987(2)
Rb(1)–O(13)	3.452(2)	Rb(2)–O(13)	3.513(2)	V(1)–O(7)	1.988(2)	V(2)–O(15)	2.083(2)
Rb(1)–O(14)	2.870(2)	Rb(2)–O(14)	3.063(2)	V(1)–O(9)	1.948(2)	V(2)–O(16)	1.616(2)
Rb(1)–O(16)	2.863(2)	Rb(2)–O(15)	3.244(2)	V(1)–O(13)	2.043(2)		
			3				
K(1)–O(2)	2.680(4)	K(2)–O(14)	2.894(4)	K(3A)–O(17D)	3.13(2)	V(1)–O(9)	1.989(4)
K(1)–O(8)	3.245(5)	K(2)–O(15A)	2.906(13)	K(3B)–O(10)	2.721(4)	V(1)–O(12)	1.954(4)
K(1)–O(11)	2.806(4)	K(2)–O(15B)	2.727(16)	K(3B)–O(16A)	2.886(15)	V(1)–O(13)	1.589(4)
K(1)–O(13)	2.812(4)	K(2)–O(16A)	2.830(13)	K(3B)–O(16B)	2.509(17)	V(2)–O(4)	1.970(4)
K(2)–O(6)	2.706(5)	K(2)–O(16B)	3.049(17)	K(3B)–O(16C)	2.419(17)	V(2)–O(5)	1.955(4)
K(2)–O(8)	2.802(4)	K(3A)–O(10)	2.696(9)	K(3B)–O(17D)	2.70(2)	V(2)–O(7)	1.977(4)
K(2)–O(9)	3.141(4)	K(3A)–O(14)	2.696(9)	K(3B)–O(17E)	2.75(2)	V(2)–O(9)	1.933(4)
K(2)–O(10)	2.949(5)	K(3A)–O(16A)	2.842(14)	V(1)–O(1)	2.024(4)	V(2)–O(14)	1.596(4)
K(2)–O(11)	2.726(4)	K(3A)–O(16B)	2.594(17)	V(1)–O(3)	2.326(4)		
K(2)–O(13)	2.988(4)	K(3A)–O(16C)	2.648(17)	V(1)–O(4)	2.052(4)		
			4				
Na(1)–O(5)	2.608(4)	Na(2)–O(2)	2.492(4)	V(1)–O(1)	2.026(3)	V(2)–O(5)	2.011(3)
Na(1)–O(6)	2.651(4)	Na(2)–O(7)	2.772(4)	V(1)–O(3)	2.252(3)	V(2)–O(10)	1.941(3)
Na(1)–O(8)	2.254(4)	Na(2)–O(8)	2.528(4)	V(1)–O(7)	1.965(3)	V(2)–O(11)	1.992(3)
Na(1)–O(17)	2.326(4)	Na(2)–O(15)	2.450(4)	V(1)–O(9)	1.947(3)	V(2)–O(15)	1.607(3)
Na(1)–O(18)	2.388(4)	Na(2)–O(19)	2.423(5)	V(1)–O(13)	1.599(3)	V(2)–O(16)	2.029(3)
Na(1)–O(19)	2.428(5)	Na(2)–O(20)	2.416(4)	V(1)–O(14)	2.064(4)		
Na(1)–O(21)	2.788(5)	Na(2)–O(21)	2.514(5)	V(2)–O(4)	2.359(3)		

Table 3. Hydrogen Bond Distances (Å) for $A_2[(VO)_2(C_4H_4O_6)(C_4H_2O_6)(H_2O)_2]\cdot(H_2O)_2$, A = Cs, 1; Rb, 2; $K_2[(VO)_2(C_4H_2O_6)_2(H_2O)_2]\cdot(H_2O)_2$, 3; and $Na_2[(VO)_2(C_4H_4O_6)(C_4H_2O_6)(H_2O)_7]\cdot(H_2O)_2$, 4

			1				
H(3A)–O(10)	1.82(2)	H(13B)–O(9)	1.74(2)	H(17A)–O(2)	2.31(3)	H(18B)–O(5)	1.985(19)
H(4A)–O(8)	1.73(2)	H(15A)–O(12)	1.931(19)	H(17B)–O(2)	2.00(3)		
H(13A)–O(17)	1.90(2)	H(15B)–O(18)	1.915(19)	H(18A)–O(10)	2.06(2)		
			2				
H(3)–O(10)	1.87(2)	H(13B)–O(9)	1.722(19)	H(17A)–O(2)	2.26(3)	H(18B)–O(5)	1.916(18)
H(4)–O(8)	1.74(2)	H(15A)–O(12)	1.882(19)	H(17B)–O(2)	2.01(2)		
H(13A)–O(17)	1.89(2)	H(15B)–O(18)	1.888(19)	H(18A)–O(10)	2.03(2)		
			3				
H(3A)–O(1)	1.82(3)	H(10A)–O(17E)	2.03(5)	H(10A)–O(3S)	1.90(4)	H(10A)–O(4S)	2.15(5)
			4				
H(3A)–O(22)	1.80(3)	H(16A)–O(10)	1.72(3)	H(18A)–O(23B)	2.19	H(21A)–O(23B)	2.06
H(4A)–O(9)	1.86(4)	H(16B)–O(22)	2.06(4)	H(18B)–O(1)	2.12	H(22A)–O(6)	1.97(3)
H(14A)–O(13)	2.07(5)	H(17A)–O(2)	1.96(3)	H(19A)–O(4)	2.07(4)	H(22B)–O(17)	1.92(3)
H(14A)–O(23B)	2.22(5)	H(17B)–O(11)	2.12(3)	H(19B)–O(23A)	2.09(4)	H(23A)–O(20)	1.88(3)
H(14B)–O(12)	1.79(3)	H(18A)–O(23A)	2.06	H(20B)–O(18)	2.00(4)	H(23B)–O(9)	1.95(3)

analyzed using a 20 kV accelerating voltage and an accumulation time of 1 min. As a qualitative measure, EDS confirmed the presence of each reported element in the title compounds.

Infrared Spectroscopy. IR spectra of ground crystals of **1**, **2**, **3**, and **4** were recorded on a PerkinElmer Spectrum 100 FT-IR spectrometer fitted with an ATR accessory in the range of 650–4000 cm^{-1}.

DOI: 10.1021/acs.inorgchem.5b00275
Inorg. Chem. 2015, 54, 4011–4020

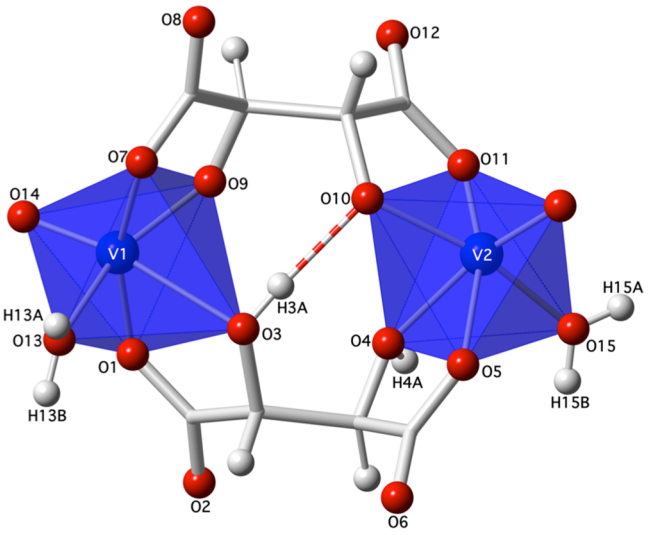

Figure 2. V_2O_{12} dimer of $A_2[(VO)_2(C_4H_4O_6)(C_4H_2O_6)(H_2O)_2]\cdot(H_2O)_2$, where A = Cs, Rb. The intracluster hydrogen bond is shown as a dashed red and white cylinder.

UV−vis Spectroscopy. UV−vis diffuse reflectance spectroscopy data of ground crystals of **1**, **2**, **3**, and **4** were obtained using a PerkinElmer Lambda 35 UV−vis scanning spectrophotometer equipped with an integrating sphere accessory in the range of 200−900 nm. Reflectance data were transformed to absorbance via the Kubelka−Munk function.

Magnetic Susceptibility. The magnetic susceptibility of **1**, **2**, **3**, and **4** were measured using a Quantum Design MPMS SQUID VSM Evercool magnetometer. The zero-field cooled (zfc) magnetic susceptibility was measured as a function of temperature between 2 and 300 K in an applied field of 1000 Oe. The measured magnetic data were corrected for shape and radial offset effects using methods reported by Morrison et al.[33]

Second Harmonic Generation. Powder SHG measurements were performed on a modified Kurtz nonlinear-optical (NLO) system using a pulsed Nd:YAG laser with a wavelength of 1064 nm. Comparisons with known SHG materials were made using ground crystalline α-SiO_2. A detailed description of the equipment and methodology has been published elsewhere.[26,34]

RESULTS AND DISCUSSION

Synthesis. A number of organic acids, such as tartaric acid, are known to reduce many transition elements under mild hydrothermal conditions and can be used as one route to obtain V^{4+} solution species in situ.[21,25,35] Separating the reduction step from the crystallization step has shown to be helpful in eliminating the formation of undesired V(V) species over desired V(IV)-containing products.[25] In addition, simple alcohols such as methanol and ethanol can be added to reactions to increase yields via decreased product solubility in solution without incorporation of the alcohol into the product. Crystals of **1**, **2**, and **3** were obtained via such a two-step hydrothermal method to avoid precipitation of alkali tartrates, which tend to crystallize much faster than the time it takes to reduce the vanadium from 5+ to 4+. To achieve formation of **1**, **2**, and **3**, the V(IV) precursor solution was created in the first step by reacting V_2O_5 with L-(+)-tartaric acid at 160 °C for 4 h. The resultant blue solution was then used as the V(IV) source material for the second step in which it was reacted with a combination of ACl and A_2CO_3, where A = Cs, Rb, and K, at only 90 °C. Initial yields of **2** and **3** were quite low; however, the addition of ethanol and methanol in step two to reduce the solubility of the dissolved reagents caused the yield to increase to ∼80%. The use of ethanol or methanol to aid in the crystallization of **1** resulted in the formation of a blue powder impurity instead of phase-pure crystals. However, even in the absence of additional alcohols, plentiful, well-faceted violet crystals of **1** were obtained with a yield of ∼75%. Attempts to crystallize a sodium compound via the same method were unsuccessful and did not yield single crystals. Slow evaporation of a sodium reaction solution over the course of 120 d produced **4** with a yield of ∼30%. Crystals of **1**, **2**, **3**, and **4** were isolated by decanting the mother liquor and collecting the crystals by filtration.

Structure. Compounds **1** and **2** are isostructural and crystallize in the chiral, orthorhombic space group $P2_12_12_1$ and exhibit a three-dimensional crystal structure consisting of distorted VO_6 octahedra and irregular AO_9/AO_{10} (A = Cs, Rb) polyhedra linked via bridging tartrate ligands that are partially deprotonated and an extensive hydrogen bonding network. Previous studies have found the protonation pattern of tartaric acid in V(IV) solutions to be pH-dependent.[36,37] The extended structure of **1** and **2** viewed along the *a*-axis is shown in Figure 3. V(1) and V(2) are located in highly distorted VO_6 octahedra with four equatorial V−O bonds of roughly the same length, one exceptionally long V−O axial bond, and one exceptionally

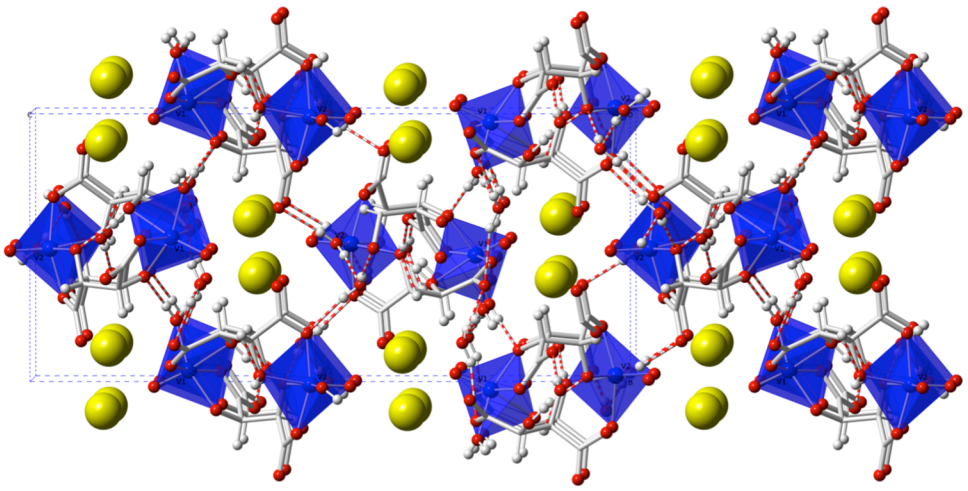

Figure 3. $A_2[(VO)_2(C_4H_4O_6)(C_4H_2O_6)(H_2O)_2]\cdot(H_2O)_2$, where A = Cs, Rb viewed down the *a* axis. Blue, gray, red, white, and yellow represent vanadium, carbon, oxygen, hydrogen, and Cs/Rb, respectively. Hydrogen bonds are shown as dashed red and white cylinders.

DOI: 10.1021/acs.inorgchem.5b00275
Inorg. Chem. 2015, 54, 4011−4020

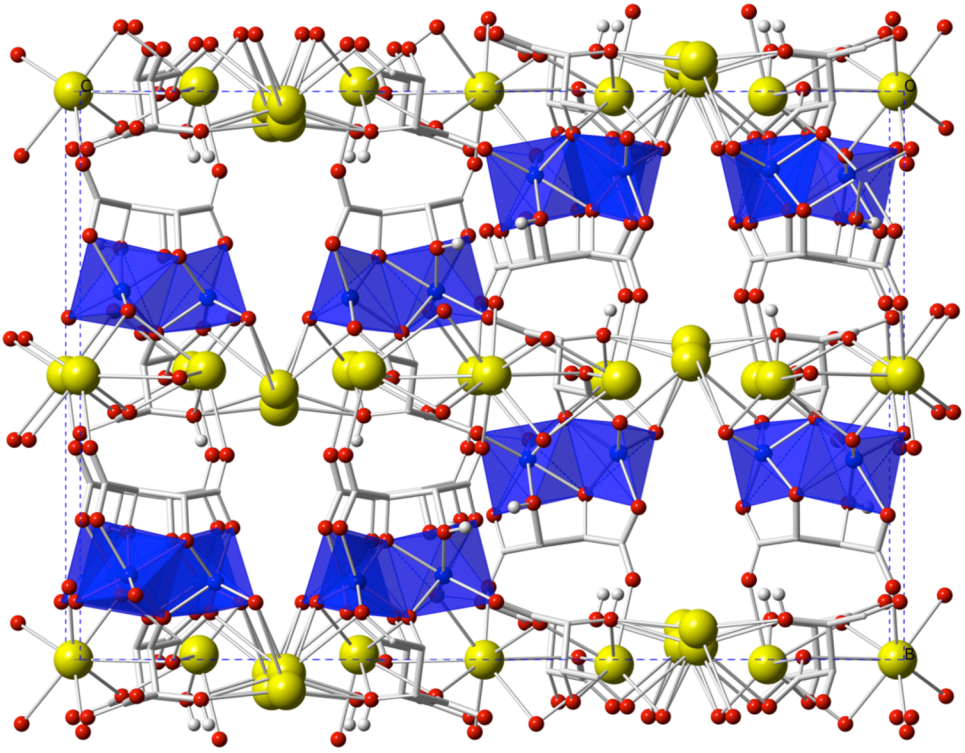

Figure 4. $K_2[(VO)_2(C_4H_2O_6)_2(H_2O)_2]\cdot(H_2O)_2$ viewed in the *bc* plane. Disordered K3A/K3B cations join double-layer K/VO/tartrate slabs into a three-dimensional framework. Blue, gray, red, white, and yellow represent vanadium, carbon, oxygen, hydrogen, and potassium, respectively. Interstitial waters reside in the cavities and are omitted for clarity.

short V−O bond. Four out of six oxygens bonded to V(1), O1, O3, O7, and O9 originate from two bidentate tartrate ligands; one, O13, originates from a monodentate water; and one, O14, originates from a bridging oxygen (oxo) atom. Four out of six oxygens bonded to V(2), O4, O5, O10, and O11 originate from two bidentate tartrate ligands; one, O15, originates from a monodentate water; and one, O16, originates from a bridging oxygen (oxo) atom. The V−O bond distances of V(1) and V(2) range from 1.606(2)−2.279(5) Å. The bidentate tartrate ligands connect the two VO_6 distorted octahedra into the dimeric unit shown in Figure 2. These dimeric units are connected to each other via Cs or Rb cations to create the extended structure shown in Figure 3. The structure contains two types of alkali cations, A(1) and A(2), (A = Cs, Rb), which are located in 9 and 10 coordinated irregular polyhedra, respectively. The Cs(1)−O and Rb(1)−O distances range from 3.013(2) to 3.753(3) Å and 2.863(2)−3.539(2) Å, respectively. The Cs(2)−O and Rb(2)−O distances range from 3.071(2) to 3.599(3) Å and 2.954(2)−3.513(2) Å, respectively. One water molecule is coordinated to A(1), and two water molecules are coordinated to A(2). All hydrogen atoms could be located on these water molecules and were refined freely. These water molecules and hydroxyl groups on the tartrate ligands give rise to an extensive hydrogen bonding network shown in Figure 3, with hydrogen bond distances ranging from 1.722(19) to 2.31(3) Å. Selected hydrogen bond distances are given in Table 3.

Compound **3** crystallizes in the orthorhombic space group $C222_1$ and exhibits a three-dimensional structure consisting of VO_6 distorted octahedra, VO_5 square pyramids, and KO_7/KO_8 irregular polyhedra linked via bridging tartrate ligands that are fully deprotonated. The extended structure of **3** viewed down the *a*-axis is shown in Figure 4. The difference in the protonation pattern of **3** accounts for the structural change

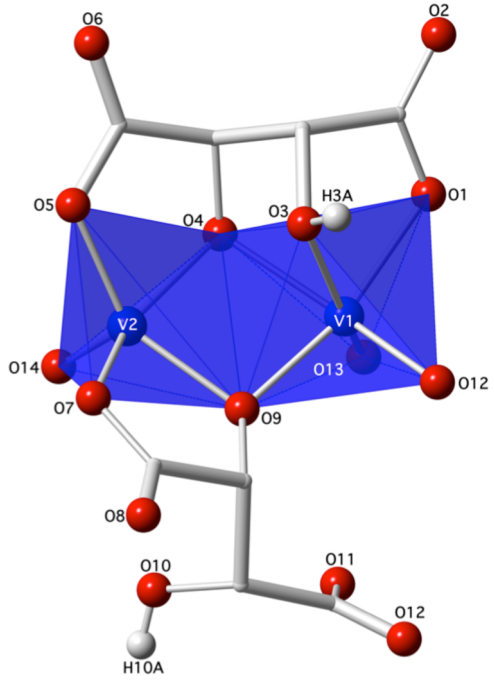

Figure 5. V_2O_9 dimer of $K_2[(VO)_2(C_4H_2O_6)_2(H_2O)_2]\cdot(H_2O)_2$.

when compared to **1** and **2**, which contain tartrate ligands that are only partially deprotonated. V(1) and V(2) are located in VO_6 distorted octahedra and VO_5 square pyramids. These polyhedra share an edge, forming unusual edge-sharing V_2O_9 dimers. Five out of six oxygens bonded to V(1), O1, O3, O4, O9, and O12 originate from a tridentate and two monodentate tartrate ligands, respectively, and one, O13, originates from a

DOI: 10.1021/acs.inorgchem.5b00275
Inorg. Chem. 2015, 54, 4011−4020

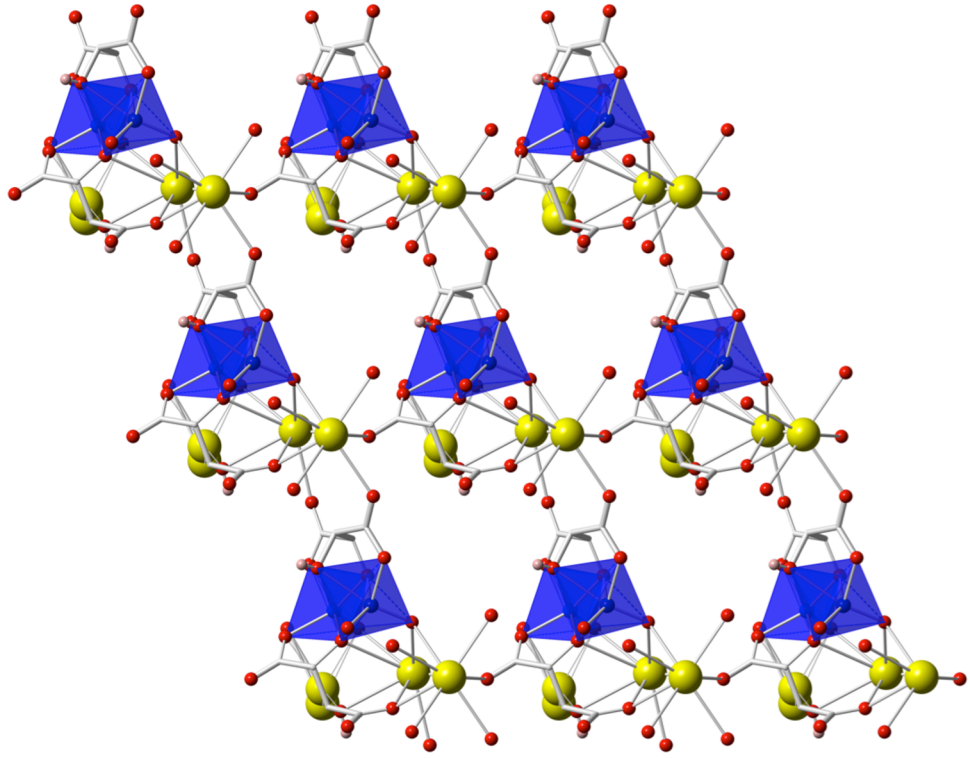

Figure 6. $K_2(VO)_2(C_4H_2O_6)_2$ cluster interconnectivity of $K_2[(VO)_2(C_4H_2O_6)_2(H_2O)_2]\cdot(H_2O)_2$ viewed in the *ab* plane. Blue, gray, red, white, and yellow represent vanadium, carbon, oxygen, hydrogen, and potassium, respectively. Interstitial waters reside in the cavities formed and are omitted for clarity.

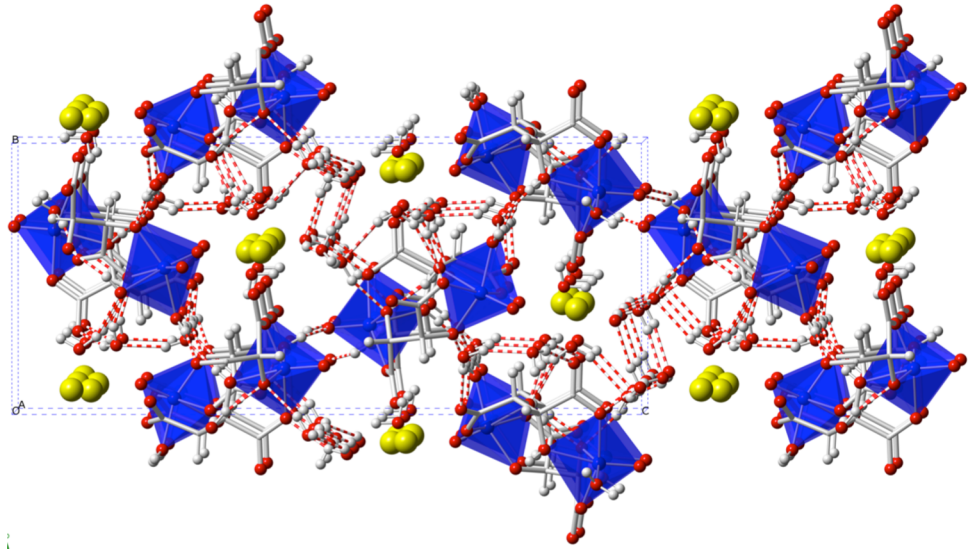

Figure 7. $Na_2[(VO)_2(C_4H_4O_6)(C_4H_2O_6)(H_2O)_7]\cdot(H_2O)_2$ viewed down the *a* axis. Blue, gray, red, white, and yellow represent vanadium, carbon, oxygen, hydrogen, and Cs/Rb, respectively. Hydrogen bonds are shown as dashed red and white cylinders.

bridging oxygen (oxo) atom. Four out of five oxygens bonded to V(2), O4, O5, O7, and O9 originate from two bidentate tartrate ligands, and one, O14, originates from a bridging oxygen (oxo) atom. The V−O bond distances on V(1) and V(2) range from 1.589(4) to 2.326(4) Å and 1.596(4)−1.977(4) Å, respectively. V(1) and V(2) polyhedra and bridging tartrate ligands form clusters shown in Figure 5. These clusters are connected via three types of potassium atoms, K1, K2, and K3A/B, which are located in one eight-coordinate and two seven-coordinate polyhedra, respectively. K1−O and K2−O distances range from 2.680(4) to 3.245(5) Å and 2.706(5)−3.184 Å, respectively. K3 is disordered over two sites with partial occupancies of 0.69(2) and 0.31(2) for K3A and K3B, respectively. K3A/B−O distances range from 2.419(17) to 3.13(2) Å. Disordered water molecules, O15−O17, and tartrate ligands are coordinated to these potassium atoms. Hydrogen atoms could not be located on the disordered water molecules. Additional disordered water molecules, O1S−O 4s, are located within cavities formed by the linkage of $K_2(VO)_2(C_4H_2O_6)_2$ clusters into a layer, which is shown in Figure 6. These layers are connected by K1 into double-layer slabs that are further connected via K3A/B to form the overall extended structure.

DOI: 10.1021/acs.inorgchem.5b00275
Inorg. Chem. 2015, 54, 4011−4020

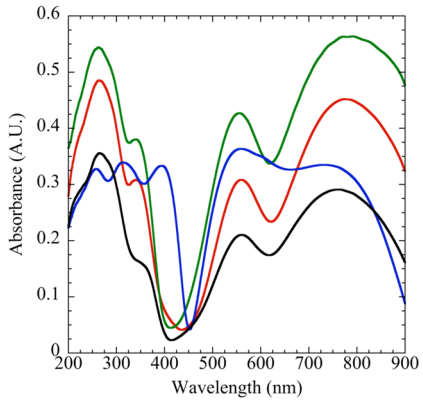

Figure 8. UV−vis data for **1**, **2**, **3**, and **4** shown in red, green, blue, and black, respectively. Three absorption maxima are observed for each compound approximately located at 375, 550, and 775 nm and can be assigned to $d_{xy} \rightarrow d_{z^2}$, $d_{xy} \rightarrow d_{x^2-y^2}$, and $d_{xy} \rightarrow d_{xz}/d_{yz}$ transitions, respectively.

Compound **4** crystallizes in the orthorhombic space group $P2_12_12_1$ and exhibits a three-dimensional structure consisting of VO_6 distorted octahedra and irregular NaO_7 polyhedra linked via bridging tartrate ligands, bridging waters, and an extensive hydrogen bonding network. The extended structure of **4** viewed along the *a*-axis is shown in Figure 5. V(1) and V(2) are located in distorted VO_6 octahedra. Four out of six oxygens bonded to V(1), O1, O3, O7, and O9 originate from two bidentate tartrate ligands; one, O14, originates from a monodentate water; and one, O13, originates from a bridging oxygen (oxo) atom. Four out of six oxygens bonded to V(2), O4, O5, O10, and O11 originate from two bidentate tartrate ligands; one, O16, originates from a monodentate water; and one, O15, originates from a bridging oxygen (oxo) atom. The V−O bond distances of V(1) and V(2) range from 1.599(3) to 2.359(3) Å. The bidentate tartrate ligands connect the two VO_6 distorted octahedra into a dimeric unit similar to dimer observed in **1** and **2**. These dimeric units are connected to each other via Na cations, water, and an extensive hydrogen bonding network to create the extended structure shown in Figure 7. The structure contains two types of alkali cations, Na(1) and Na(2), which are located in seven-coordinated irregular polyhedra. The Na(1)−O and Na(2)−O distances range from 2.254(4) to 2.788(5) Å and 2.416(4)−2.772(4) Å, respectively. Four water molecules are coordinated to Na(1), and three water molecules are coordinated to Na(2). All hydrogen atoms could be located on these water molecules and were refined freely. These water molecules and hydroxyl groups on the tartrate ligands give rise to an extensive hydrogen bonding network shown in Figure 7, with hydrogen bond distances ranging from 1.80(3) to 2.22(5) Å. Selected hydrogen bond distances are given in Table 3.

Infrared Spectroscopy. The IR spectra for **1**, **2**, **3**, and **4**, which are shown in the Supporting Information, Figure S2, were collected between 650 and 4000 cm^{-1}. The broad band observed in the 3200−3600 cm^{-1} region is characteristic for O−H vibrations of water molecules and hydroxyl groups. The presence of tartrate groups produces vibrations of C−O, C−C, C−O−O. The expected bending mode of water at ∼1600 cm^{-1} overlaps with the intense C−O stretching mode of the tartrate group. The bands in the region of 1200−1450 cm^{-1} are attributed to the symmetric stretching modes of the tartrate C−O bonds, and the remainder of the bands observed below

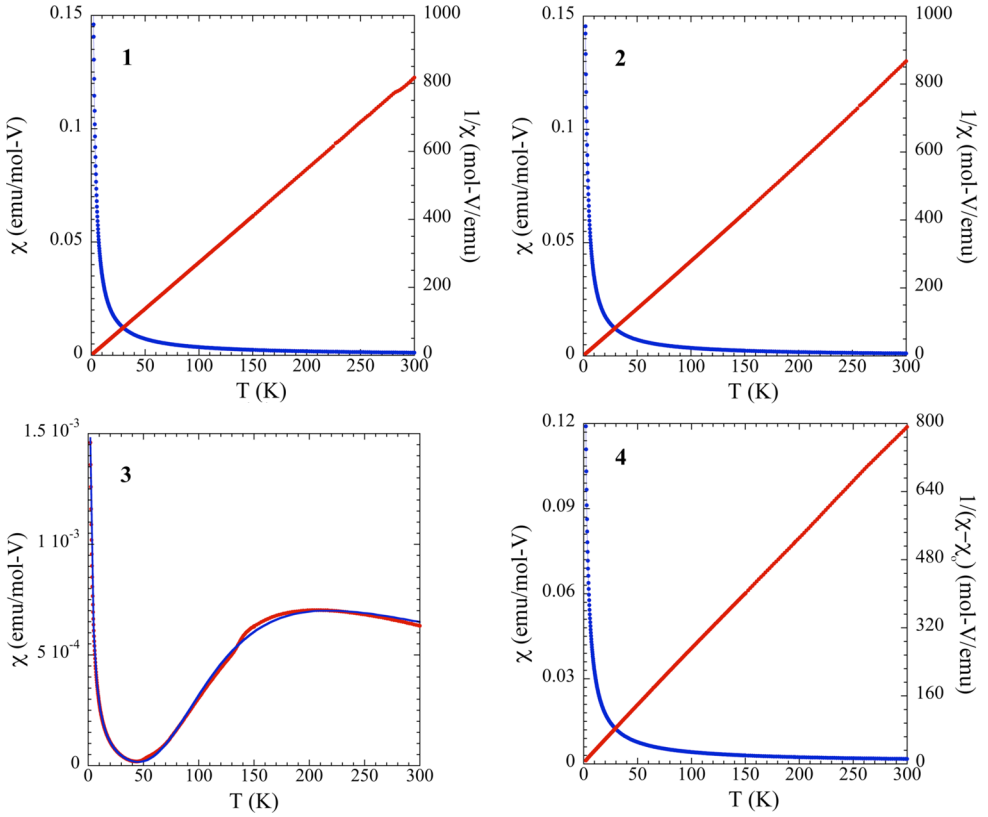

Figure 9. Magnetic susceptibility plots of **1**, **2**, **3**, and **4**. χ and $1/\chi$ are shown in blue and red, respectively, for **1**, **2**, and **4**. For **3**, χ and a fit to the data using the Bleaney−Bowers equation for isolated dimers are shown in blue and red, respectively.

DOI: 10.1021/acs.inorgchem.5b00275
Inorg. Chem. 2015, 54, 4011−4020

1000 cm^{-1} can be assigned to V−O, C−C, and C−O−O vibrational modes.[20,21,38−40]

UV−vis and Magnetism. UV−vis absorbance data shown in Figure 8 were collected using ground crystals of **1**, **2**, **3**, and **4**. Vanadium in the +4 oxidation state has a d^1 electron configuration, and a transition from the $^2T_{2g}$ ground state to the ^2E_g excited state is expected. Three absorption maxima are observed for each compound approximately located at 375, 550, and 775 nm and can be assigned to $d_{xy} \rightarrow d_{z^2}$, $d_{xy} \rightarrow d_{x^2-y^2}$, and $d_{xy} \rightarrow d_{xz}/d_{yz}$ transitions, respectively.[41,42] The unpaired electrons in **1**, **2**, **3**, and **4** can be observed in magnetic susceptibility measurements. The temperature dependences of the magnetic susceptibilities of **1**, **2**, **3**, and **4** measured in an applied field of 1000 Oe, are shown in Figure 9. In **1**, **2**, and **4** the distorted VO_6 octahedra are separated by the bridging tartrate ligands and, due to the long V−V separation, no magnetic coupling is expected or observed. Down to 2 K, the data do not reveal any long-range magnetic order and follow the Curie−Weiss (C−W) law as expected for simple paramagnetic species. The magnetic moments calculated from the inverse susceptibilities are 1.71, 1.72, and 1.75 μ_B for **1**, **2**, and **4**, respectively, which are in good agreement with the expected value of 1.73 μ_B for a $3d^1$ spin-only system.[43] The magnetic property of **3**, however, is quite different from the other members, as expected considering its crystal structure in which edge-shared V_2O_9 dimers are present. Since there was no significant difference between zfc and fc data, only zfc data are shown for the purpose of discussion. The broad maximum in the susceptibility data, observed at ∼180 K, is indicative of spin coupling within the vanadium dimers in this compound, whereas the sharp increase at low temperature is likely due to the presence of a small amount of a paramagnetic impurity. Considering the crystal structure of **3**, one would expect that the magnetic interactions between the V^{4+} ions within the dimer would dominate the magnetic data and that magnetic coupling between dimers, due to their long physical separation, would not be observed. Such a spin one-half dimer system is perhaps the simplest low-dimensional magnetic system exhibiting a spin-gap between the ground and excited states.[44−46] To better understand the magnetism of **3**, we modeled the magnetic susceptibility data using the modified Bleaney−Bowers equation,[47−49] which can be written as

$$\chi_M = \frac{N_A \mu_B^2 g^2}{\kappa_B T(3 + E^{-2J/\kappa_B T})} + \frac{C}{T - \theta} + \chi_{TIP} \quad (1)$$

where N_A, g, μ_B, k_B, and J are Avogadro's number, g-factor, Bohr-magneton, Boltzmann constant, and the intradimer exchange coupling constant, respectively. The second C−W term corrects for contributions from trace amount of impurities that are sometimes observed in the very low-temperature regime, and χ_{TIP} is the temperature-independent paramagnetic susceptibility. The best fit generated values of g = 1.89, J/k_B = −177 K, and $\chi_{TIP} = -7.65 \times 10^{-5}$ emu/mol. The negative J value implied an antiferromagnetic interaction within the dimers, which is expected based on the dimer bridging angles (V−O−V) of 100.0(2) and 96.7(2). The magnetic property of **3** appears well-described by the isolated spin-half dimer model.

Second Harmonic Generation. All materials that crystallize in one of the non-centrosymmetric crystal classes, except 432, may exhibit SHG behavior. Although **1**, **2**, **3**, and **4** belong to this class, only very weak behavior was observed for **1**, **2**, and **3**; most likely because these compounds exhibit only a very small dipole moment. The spherical-like coordination environments of the alkali cations and opposing orientation of polar axial V−O bonds in VO_6 polyhedra of the dimers account for the small magnitude of the dipole moment. Large SHG efficiency is typically correlated with large dipole moments.[50−52] All compounds exhibit nonphase-matching behavior with an SHG efficiency of ∼1× α-SiO_2, shown in Figure 10. Compound **4** could not be tested due to insufficient sample size and the impracticality of creating more given the time it takes to crystallize **4**.

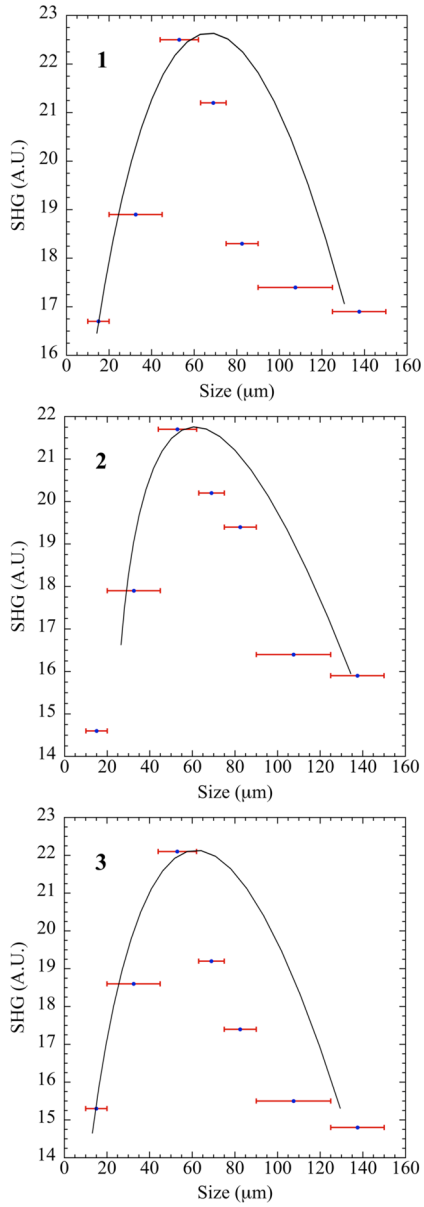

Figure 10. Size-dependent SHG response of **1**, **2**, and **3**. Uncertainty is shown as red error bars. Black curves were added to help guide the eye when interpreting the behavior.

CONCLUSION

We have successfully synthesized and characterized four new oxovanadium(IV) tartrate hybrid compounds, $A_2[(VO)_2(C_4H_4O_6)(C_4H_2O_6)(H_2O)_2]\cdot(H_2O)_2$, where A = Cs; Rb; $K_2[(VO)_2(C_4H_2O_6)_2(H_2O)_2]\cdot(H_2O)_2$; and $Na_2[(VO)_2(C_4H_4O_6)(C_4H_2O_6)(H_2O)_7]\cdot(H_2O)_2$, utilizing a two-step, mild hydrothermal technique and slow evaporation. Vanadium in these structures is in the +4 oxidation state. By varying the size of the alkali cation three different structure types can be formed.

DOI: 10.1021/acs.inorgchem.5b00275
Inorg. Chem. 2015, 54, 4011−4020

Structures **1**, **2**, and **4** formed for A = Cs, Rb, and Na and have dimers with long V−V vanadium distances and exhibit simple paramagnetic behavior, while structure **3**, which forms for A = K, contains isolated dimers with short V−V separations that give rise to spin-dimer behavior due to antiferromagnetic coupling between the V^{4+} ions.

■ ASSOCIATED CONTENT

Supporting Information

CIF files, PXRD patterns, and IR spectra. This material is available free of charge via the Internet at http://pubs.acs.org.

■ AUTHOR INFORMATION

Corresponding Author

*E-mail: zurloye@mailbox.sc.edu.

Notes

The authors declare no competing financial interest.

■ ACKNOWLEDGMENTS

Financial support for this work was provided by the National Science Foundation under DMR-1301757 and is gratefully acknowledged. Support for magnetic measurements was provided by a grant from the U.S. Department of Energy, Office of Basic Energy Studies, Materials Sciences and Engineering Division, under Grant No. DE-SC-0001061 and is gratefully acknowledged.

■ REFERENCES

(1) Djerdj, I.; Cao, M.; Rocquefelte, X.; Ćerný, R.; Jagličić, Z.; Arčon, D.; Potočnik, A.; Gozzo, F.; Niederberger, M. *Chem. Mater.* **2009**, *21*, 3356−3369.

(2) Marino, N.; Lloret, F.; Julve, M.; Doyle, R. P. *Dalton Trans.* **2011**, *40*, 12248−12256.

(3) Yan, B.; Luo, J.; Dube, P.; Sefat, A. S.; Greedan, J. E.; Maggard, P. A. *Inorg. Chem.* **2006**, *45*, 5109−5118.

(4) Yan, B.; Maggard, P. A. *Inorg. Chem.* **2007**, *46*, 6640−6646.

(5) Park, D. H.; Cheng, C.-F.; He, H.; Klinowski, J. *J. Mater. Chem.* **1997**, *7*, 159−162.

(6) Santamaría-González, J.; Luque-Zambrana, J.; Mérida-Robles, J.; Maireles-Torres, P.; Rodríguez-Castellón, E.; Jiménez-López, A. *Catalysis* **2000**, *68*, 67−73.

(7) Scheurell, K.; Hoppe, E.; Brzezinka, K.-W.; Kemnitz, E. *J. Mater. Chem.* **2004**, *14*, 2560−2568.

(8) Taufiq-Yap, Y. H.; Rownaghi, A. A.; Hussein, M. Z.; Irmawati, R. *Catal. Lett.* **2007**, *119*, 64−71.

(9) Chernova, N. A.; Roppolo, M.; Dillon, A. C.; Whittingham, M. S. *J. Mater. Chem.* **2009**, *19*, 2526−2552.

(10) Koffer, J. H.; Olshansky, J. H.; Smith, M. D.; Hernandez, K. J.; Zeller, M.; Ferrence, G. M.; Schrier, J.; Norquist, A. J. *Cryst. Growth Des.* **2013**, *13*, 4504−4511.

(11) Pralong, V.; Caignaert, V.; Raveau, B. *J. Mater. Chem.* **2011**, *21*, 12188−12201.

(12) Whittingham, M. S. *Chem. Rev.* **2004**, *104*, 4271−4302.

(13) Tengku Azmi, T. S. M.; Yusoff, A. R. M.; Abdul Karim, K. J. *Chromatographia* **2010**, *72*, 141−144.

(14) Zhang, X.-M.; Tong, M.-L.; Lee, H. K.; Chen, X.-M. *J. Solid State Chem.* **2001**, *160*, 118−122.

(15) Blakely, C. K.; Bruno, S. R.; Poltavets, V. V. *Inorg. Chem.* **2011**, *50*, 6696−6700.

(16) Kiss, T.; Buglyó, P.; Sanna, D.; Micera, G.; Decock, P.; Dewaele, D. *Inorg. Chim. Acta* **1995**, *239*, 145−153.

(17) Polinski, M. J.; Cross, J. N.; Villa, E. M.; Lin, J.; Alekseev, E. V.; Depmeier, W.; Albrecht-Schmitt, T. E. *Inorg. Chem.* **2013**, *52*, 8099−8105.

(18) Tsang, C. F.; Manthiram, A. *J. Mater. Chem.* **1997**, *7*, 1003−1006.

(19) Tsang, C. F.; Kim, J.; Manthiram, A. *J. Mater. Chem.* **1998**, *8*, 425−428.

(20) Yeon, J.; Smith, M. D.; Sefat, A. S.; zur Loye, H.-C. *Inorg. Chem.* **2013**, *52*, 2199−2207.

(21) Yeon, J.; Sefat, A. S.; Tran, T. T.; Halasyamani, P. S.; zur Loye, H.-C. *Inorg. Chem.* **2013**, *52*, 6179−6186.

(22) García-Jaca, J.; Pizarro, J. L.; Larramendi, J. I. R.; Lezama, L.; Arriortua, M. I.; Rojo, T. *J. Mater. Chem.* **1995**, *5*, 277−283.

(23) Wrobleski, J. T.; Thompson, M. R. *Inorg. Chim. Acta* **1988**, *150*, 269−277.

(24) Schwendt, P.; Tracey, A. S.; Tatiersky, J.; Gáliková, J.; Žák, Z. *Inorg. Chem.* **2007**, *46*, 3971−3983.

(25) Abeysinghe, D.; Smith, M. D.; Yeon, J.; Morrison, G.; zur Loye, H.-C. *Cryst. Growth Des.* **2014**, *14*, 4749−4758.

(26) Ok, K. M.; Chi, E. O.; Halasyamani, P. S. *Chem. Soc. Rev.* **2006**, *35*, 710−717.

(27) *SMART Version 5.630, SAINT+ Version 6.45 and SADABS Version 2.10;* Bruker Analytical X-ray Systems, Inc.: Madison, WI, 2003.

(28) Sheldrick, G. M. *Acta Crystallogr., Sect. A: Found. Crystallogr.* **2008**, *64*, 112−122.

(29) Dolomanov, O. V.; Bourhis, L. J.; Gildea, R. J.; Howard, J. A. K.; Puschmann, H. *J. Appl. Crystallogr.* **2009**, *42*, 339−341.

(30) Brese, N. E.; O'Keeffe, M. *Acta Crystallogr., Sect. B: Struct. Crystallogr. Cryst. Chem.* **1991**, *47*, 192−197.

(31) Brown, I. D.; Altermatt, D. *Acta Crystallogr., Sect. B: Struct. Crystallogr. Cryst. Chem.* **1985**, *41*, 244−247.

(32) Compound 1, V1:4.14 V2:4.09; Compound 2, V1:4.12 V2:4.09; Compound 3, V1:4.14 V2:4.16; Compound 4, V1:4.17 V2:4.10.

(33) Morrison, G.; zur Loye, H.-C. *J. Solid State Chem.* **2015**, *221*, 334−337.

(34) Kurtz, S. K.; Perry, T. T. *J. Appl. Phys.* **1968**, *39*, 3798−3813.

(35) Hamdouni, M.; Walha, S.; Kabadou, A.; Duhayon, C.; Sutter, J.-P. *Cryst. Growth Des.* **2013**, *13*, 5100−5106.

(36) Dyachkova, T. A.; Glebov, A. N.; Budnikov, G. K.; Tarasov, O. Y.; Sal-nikov, Y. I. *Koord. Khim.* **1990**, *16*, 1227−1229.

(37) Glebov, A. N.; Sal'nikov, Y. I.; Tarasov, O. Y. *Koord. Khim.* **1988**, *45*, 655−660.

(38) Davis, J. M. *J. Chem. Educ.* **1968**, *45*, 473.

(39) Deacon, G. B.; Phillips, R. J. *Coord. Chem. Rev.* **1980**, *33*, 227−250.

(40) Frederickson, L. D., Jr.; Hausen, D. M. *Anal. Chem.* **1963**, *35*, 818−827.

(41) Ballhausen, C. J.; Gray, H. B. *Inorg. Chem.* **1962**, *1*, 111−122.

(42) Kumar, P.; Gupta, M.; Lal, K. M. *Asian J. Phys.* **1995**, *4*, 205−206.

(43) Blundell, S. *Magnetism in Condensed Matter;* Oxford University Press: Oxford, U.K., 2001.

(44) Camara, I. S.; Gautier, R.; Le Fur, E.; Trombe, J.-C.; J, G.; Ghorayeb, A. M.; Stepanov, A. *Phys. Rev. B: Condens. Matter Mater. Phys.* **2010**, *81*, 184433.

(45) Isobe, M.; Ueda, Y. *J. Phys. Soc. Jpn.* **1996**, *65*, 3142−3145.

(46) Mur, J.; Darriet, J. *C. R. Acad. Sci., Ser. II: Mec., Phys., Chim., Sci. Terre Univers* **1985**, *300*, 599−602.

(47) Bleaney, B.; Bowers, K. D.; Ingram, D. J. E. *Proc. R. Soc. London, Ser. A* **1955**, *228*, 147−157.

(48) Kahn, O. *Molecular Magnetism;* VCH Publishers: New York, 1993.

(49) Lahti, P. M. *Magnetic Properties of Organic Materials;* Marcel Dekker, Inc.: New York, 1999; pp 558.

(50) Kim, S.-H.; Yeon, J.; Halasyamani, P. S. *Chem. Mater.* **2009**, *21*, 5335−5342.

(51) Nguyen, S. D.; Yeon, J.; Kim, S.-H.; Halasyamani, P. S. *J. Am. Chem. Soc.* **2011**, *133*, 12422−12425.

(52) Yeon, J.; Kim, S.-H.; Nguyen, S. D.; Lee, H.; Halasyamani, P. S. *Inorg. Chem.* **2012**, *51*, 2662−2668.

DOI: 10.1021/acs.inorgchem.5b00275
Inorg. Chem. 2015, 54, 4011−4020